An infrared scattering by evaporating droplets at the initial stage of a pool fire suppression by water sprays

Leonid A. Dombrovsky, Siaka Dembele, Jennifer X. Wen

PII: S1350-4495(18)30060-4
DOI: https://doi.org/10.1016/j.infrared.2018.03.027
Reference: INFPHY 2530

To appear in: *Infrared Physics & Technology*

Received Date: 30 January 2018
Revised Date: 28 March 2018
Accepted Date: 29 March 2018

Please cite this article as: L.A. Dombrovsky, S. Dembele, J.X. Wen, An infrared scattering by evaporating droplets at the initial stage of a pool fire suppression by water sprays, *Infrared Physics & Technology* (2018), doi: https://doi.org/10.1016/j.infrared.2018.03.027

An infrared scattering by evaporating droplets at the initial stage of a pool fire suppression by water sprays

Leonid A. Dombrovsky [a, b], Siaka Dembele [a], and Jennifer X. Wen [c]

[a] Depart. of Mechanical & Automotive Engineering, Kingston University, London, SW15 3DW, UK
[b] Tyumen State University, 6 Volodarsky St., Tyumen, 625003, Russia
[c] School of Engineering, University of Warwick, Coventry CV4 7AL, UK

Abstract

The computational analysis of downward motion and evaporation of water droplets used to suppress a typical transient pool fire shows local regions of a high volume fraction of relatively small droplets. These droplets are comparable in size with the infrared wavelength in the range of intense flame radiation. The estimated scattering of the radiation by these droplets is considerable throughout the entire spectrum except for a narrow region in the vicinity of the main absorption peak of water where the anomalous refraction takes place. The calculations of infrared radiation field in the model pool fire indicate the strong effect of scattering which can be observed experimentally to validate the fire computational model.

Keywords: Suppression of pool fires; Evaporating water droplets; Thermal radiation, Strong infrared scattering.

Nomenclature

a	radius of droplet
c	specific heat capacity
D	radiation diffusion coefficient
C_D	drag coefficient
f_v	volume fraction of droplets
E	normalized coefficient
G	spectral irradiation
g	acceleration of gravity
I	radiation intensity
K	coefficient introduced by Eq. (6b)
k	thermal conductivity
L	latent heat of evaporation
m	complex index of refraction
n	index of refraction
Q	efficiency factor
r	radial coordinate
S	source function
u	velocity
W	generated radiation power
w	normalized radiation power
x	diffraction (size) parameter
z	axial coordinate

Greek symbols

α, β	absorption and extinction coefficients
γ	coefficient introduced by Eq. (6b)
ε	emissivity
η	dynamic viscosity
κ	index of absorption
λ	wavelength
ξ	coefficient in Eq. (11)
ρ	density
σ	scattering coefficient
ψ	coefficient introduced by Eq. (6b)
χ	eigenvalue introduced by Eq. (9b)
$\vec{\Omega}$	unit vector of direction

Subscripts

0	initial value	r	radiative
a	absorption	ref	referred
b	blackbody	s	scattering
d	droplet	sat	saturation
g	gas	t	total
max	maximum	tr	transport
		w	water, wall

1. Introduction

The complex behaviour of water sprays used in suppression of pool fires is an important engineering problem [1–5]. Strictly speaking, one should take into account the effect of water sprays on flow field parameters. It is really important in the regular regime of fire suppression. Following [6], a preliminary probe stage of the fire suppression with a very small flow rate of water is considered. Obviously, the effect of a low flow rate water spray on the fire parameters at the probe stage is negligible. It means that one can consider the motion, heating, and evaporation of single water droplets in the flame without taking into account any feedback effects. It is also assumed that a relatively thin water spray moves down parallel to the flame axis. This approach is convenient to focus on the most important special features of the droplet behaviour at the probe stage. Of course, a simplified model for droplet motion and evaporation is insufficient to obtain accurate results for the interaction of a fast developing turbulent fire and water droplets. The latter is especially important when the characteristic times of the flow field changes and displacement of the droplets are comparable with each other.

In the limit of a relatively slow variation of the flow field, the evaporation of droplets accompanied by a decrease in their velocity may lead to a significant volume fraction of small droplets at several specific local areas. In the reality, both the position and parameters of these local areas in the developing flame are changed rather rapidly.

It is known that small water droplets are characterized by a strong scattering of light at the wavelength comparable with the droplet size [7]. This optical effect, which is commonly observed in the visible for the natural mists, has been recently considered as a promising way to improve shielding of fire radiation by multi-layered water sprays [8, 9]. It is important that the gaseous combustion products in the fire do not scatter the radiation. The radiation scattering by soot aggregates in the infrared range is also negligible (a considerable scattering by soot aggregates can be observed in the visible range only) [10–13]. As a result, one can observe local regions of small water droplets near the flame axis because of their infrared scattering. This may be a scattering of the flame self-emission, but one can also use an external irradiation.

The objective of this paper is two-fold: (1) to study the behaviour of moving water droplets which can be collected in some local areas of the flame before their total evaporation and (2) to estimate the effect of scattering of the flame infrared radiation by these small droplets on the radiation source function, which is responsible for the observed flame emission.

It seems natural to consider first the typical trajectories and evaporation dynamics of water droplets to find the local regions where the volume fraction of highly scattering small droplets is expected to be significant.

2. Motion and evaporation of water droplets

The interaction of water sprays with fires has been modelled computationally in many papers especially during the last two decades [14–18]. However, there is no need to discuss here the state-of-the-art in this field because the present paper is focused on another particular problem. At the probe stage of the fire suppression, one can supply only the droplets falling down not far from the flame axis. For simplicity, the spherical water droplets are assumed to have the same radius at the initial cross section of the spray. It is sufficient to consider a few selected trajectories of droplets falling initially along the flame axis without any interactions between the droplets. According to [16, 19], the following sets of equations are derived for the droplet motion:

$$\frac{dz_\mathrm{d}}{dt} = u_\mathrm{d} \qquad z_\mathrm{d}(0) = z_0 \tag{1a}$$

$$\frac{du_\mathrm{d}}{dt} = \frac{3C_\mathrm{D}}{8a}\frac{\rho}{\rho_\mathrm{w}}\left(u_\mathrm{g} - u_\mathrm{d}\right)\left|u_\mathrm{g} - u_\mathrm{d}\right| - g \qquad u_\mathrm{d}(0) = -u_{\mathrm{d}0} \tag{1b}$$

$$C_\mathrm{D} = 24\left(1 + 0.15\,\mathrm{Re}_\mathrm{d}^{0.687}\right)/\mathrm{Re}_\mathrm{d} \qquad \mathrm{Re}_\mathrm{d} = 2\rho\left|u - u_\mathrm{d}\right|a/\eta \tag{1c}$$

where the subscripts “g”, “d” and “w” refer to the gaseous medium, droplet and water, u is the velocity, a is the droplet radius, C_D is the drag coefficient, Re is the Reynolds number. It is assumed that water droplets are first heated up to the saturation temperature without evaporation (at $0 < t < t_\mathrm{sat}$):

$$\frac{dT_\mathrm{d}}{dt} = \frac{1.5\mathrm{Nu}\,k}{\rho_\mathrm{w} c_\mathrm{w} a^2}\left(T_\mathrm{g} - T_\mathrm{d}\right) \qquad T_\mathrm{d}(0) = T_0 \qquad t < t_\mathrm{sat} \tag{2a}$$

$$\mathrm{Nu} = 2 + 0.6\,\mathrm{Re}_\mathrm{d}^{1/2}\,\mathrm{Pr}^{1/3} \qquad \mathrm{Pr} = \eta c/k \tag{2b}$$

(Nu and Pr are the Nusselt and Prandtl numbers) and then evaporated according to the following simple equation (at $t > t_\mathrm{sat}$):

$$\frac{da}{dt} = -\mathrm{Nu}\,\frac{k\left(T_\mathrm{g} - T_{\mathrm{w,sat}}\right)}{2a\rho_\mathrm{w} L_\mathrm{w}} \qquad a\left(t_\mathrm{sat}\right) = a_0 \qquad t > t_\mathrm{sat} \tag{3}$$

where L_w is the latent heat of evaporation of water. A similar model has been recently used in analysis of water mist curtains [8, 9]. This simplified evaporation model is also sufficient

for qualitative estimates of the present paper because of very fast heating of moving droplets and large molar fraction of water vapour in the flame. It is not necessary at the moment to consider sophisticated evaporation models like that developed in paper [20]. A transfer from the droplet heating to its evaporation is given by equation:

$$T_{\mathrm{d}}(t_{\mathrm{sat}}) = T_{\mathrm{w,sat}} \tag{4}$$

In contrast to recent papers [3, 4, 21], the effects of thermal radiation are neglected in the above model as compared with convective heat transfer from ambient hot gases. This assumption can be revised on the basis of the radiation field calculations. Obviously, the local relative volume fraction of water droplets can be calculated as follows:

$$\bar{f}_{\mathrm{v}} = f_{\mathrm{v}} / f_{\mathrm{v0}} = (u_{\mathrm{d0}} / u_{\mathrm{d}})(a/a_0)^3 \tag{5}$$

Equation (5) indicates that the volume fraction of water droplets decreases with their evaporation, but a strong increase in the volume fraction can be observed in the regions of slowly moving droplets.

3. Application Case Study

A pool fire is defined as a turbulent diffusion flame burning above a horizontal pool of vaporising fuel (e.g. liquid) where the fuel has zero or low initial momentum. Such fires are dominated by buoyancy since the velocity and momentum of the fuel vapour leaving the pool surface are negligible. In order to reproduce pool fires in laboratory conditions, most fire researchers used gas burners constructed of porous refractory material, where the gas fuel is supplied at very low velocity under controlled burning. Controlling the mass burning rate is a way to quantify with certainty the heat release rate which is an important quantity in pool fire studies. Moreover, bearing in mind that flaming combustion only occurs in the gas phase, this case also mimics the realistic scenario of a pool of liquid fuel with a low momentum vapour fuel initially formed at the surface of the pool before combusting with oxygen. In the present study, a methane gas burner is employed to replicate typical experimental condition of a burning liquid pool fire. This is common practice in CFD simulation of pool fires.

The flame is burning in the open quiescent environment with a heat release rate of 53 kW. The numerical results of a CFD simulation from paper [6] for the transient flame at time moment $t = 1\mathrm{s}$ are considered as the case problem. The calculated transient flame is three-dimensional, but deviations of the main parameters from the axisymmetric case are not significant. Following [6], the axisymmetric model flame used in calculations was obtained by angular averaging of all parameters. The data for gas temperature and axial component of gas velocity in the flame are presented in Fig. 1. The temperature field appears to be strongly non-uniform and contains a very hot circular region in a vicinity of a ring with radius about 8 cm in the forward part of the flame, at $z = 0.4\mathrm{m}$. This hot region moves upward with a relatively high speed of about 4 m/s (Fig. 1b). On the contrary, there is a cold and slowly

moving region of a gas at the axis of the flame at $z > 0.3\,\mathrm{m}$. Moreover, a downward motion of a gas is observed in this central region. The above described specific structure of the flame was a motivation of subsequent attention to both the cold central region and the circular hot and high-velocity region of the flame.

We have considered the developing flame at several time moments, but the selected flame appeared to be the most interesting because of two sub-regions with quite different local temperatures and axial velocities shown in Fig. 1. This specific flame is convenient to analyze the behavior of water droplets at very different conditions.

The temperature $T_0 = 300\,\mathrm{K}$ was taken for water droplets at the initial cross section $z_0 = 0.5\,\mathrm{m}$ of the water spray. As to the droplet size and initial velocity, a set of various realistic values of these quantities was considered. Some computational results including those obtained in [6] are presented in Fig. 2. The behaviour of water droplets moving along two parallel lines appeared to be quite different. However, the trajectories of evaporating droplets of different initial size are focused in small local areas. In the case of droplets moving along the axis, their initial velocity makes no difference because of a relatively small relaxation time (Fig. 2a). The evaporation of these droplets will be completed due to absorption of thermal radiation from a surrounding flame. On the contrary, the large droplets supplied at $r_0 = 0.1\mathrm{m}$ with relatively high initial velocity can penetrate to the hot region and totally evaporate during their backward motion (Fig. 2b).

According to Figs. 2a and 2b, all the trajectories of droplets can be subdivided into three parts: (1) the straightforward falling down without any considerable changes in the droplet size, (2) the considerable evaporation accompanied by a decrease of the droplet velocity up to zero value, and (3) the return motion of the continuously evaporating droplet up to the relatively stable position in a cold and slowly moving gas when both the evaporation rate and the droplet velocity are close to zero. It is interesting that the area of the final focusing of small and almost immovable droplets appeared to be the same for droplets of quite different initial radius. The volume fraction of small evaporating droplets may be very high in the local areas of their collection and almost total evaporation. Of course, the assumption of independently moving droplets is incorrect in the vicinity of these areas. It is a serious problem which does not have a simple solution at the moment [19]. This is one of the important reasons of a qualitative character of physical estimates of the present paper. However, there is no doubt in the main physical result of this section: the small partially evaporated water droplets are focused in several local areas at the front surface of the developing pool fire.

One should recall that the above result was obtained by ignoring the effects of turbulence and also time variation of the Reynolds-averaged flow field of developing flames. Obviously, the turbulence cannot affect the motion of inertial particles at high values of the Stokes number, which is proportional to the square of the droplet radius [19]. It is also interesting that turbulence can not only mitigate the particle collection. On the contrary, the transient effect of the so-called "preferential concentration" of particles with Stokes number about unity may be significant even in the homogeneous and isotropic turbulence [22–24].

The effect of a fast time variation of the developing flame parameters is expected to be much stronger than the effect of turbulence. Additional CFD calculations have shown that a characteristic time of considerable variations of the flow field shown in Fig. 1 is about 0.1–0.2 s. It means that the shape of the local areas with high volume fraction of small water droplets may be deformed and shifted at the probe suppression stage. More definite conclusion about the behavior of these local areas depends on the increase of water flow rate while transfer to the regular fire suppression.

In all cases, the moving local areas containing small evaporating droplets will lead to the infrared scattering by these small water droplets.

4. Infrared properties of water droplets

The spectral optical constants, n and κ, of pure water are well known from early papers [25, 26]. For convenience of subsequent analysis, spectral dependences of these quantities in the most important part of the infrared range are presented in Fig. 3. The spectral characteristics of absorption and scattering of spherical water droplets can be calculated using the Mie theory [27–29]. Two dimensionless far-field characteristics which can be obtained from the analytical Mie solution are used in the calculations of the present paper: the efficiency factor of absorption, Q_{a}, and the transport efficiency factor of scattering, $Q_{\mathrm{s}}^{\mathrm{tr}}$. According to the Mie theory, the values of Q_{a} and $Q_{\mathrm{s}}^{\mathrm{tr}}$ depend on both the complex index of refraction $m = n - \mathrm{i}\kappa$ and the diffraction (size) parameter $x = 2\pi a/\lambda$, where a is the droplet radius. The exact Mie calculations are time-consuming, especially for large droplets with $x >> 1$. Therefore, as it was done in recent studies [8, 9], we use the following analytical approximation suggested in [30] for semi-transparent particles:

$$Q_{\mathrm{a}} = \frac{4n}{(n+1)^2}\left[1 - \exp(-4\kappa x)\right] \qquad Q_{\mathrm{s}}^{\mathrm{tr}} = K\begin{cases} \psi/5 & \text{when } \psi \le 5 \\ (5/\psi)^{\gamma} & \text{when } \psi > 5 \end{cases} \tag{6a}$$

$$K = 1.5n(n-1)\exp(-15\kappa) \qquad \gamma = 1.4 - \exp(-80\kappa) \qquad \psi = 2x(n-1) \tag{6b}$$

A comparison of approximation (6 a, b) with Mie theory calculations for water droplets at two typical infrared wavelengths can be found in paper [8]. As one can expect, the approximate relations are sufficiently accurate for both Q_a and Q_s^{tr} in the spectral range of a weak absorption. As to water absorption band at wavelength of $\lambda = 3\,\mu m$, only the approximation for the absorption efficiency factor is important because $Q_s^{tr} << Q_a$. The latter is typical of the narrow region of anomalous refraction [31, 32].

The so-called monodisperse approximation, when all the droplets are assumed to have the same radius in the initial cross section of the spray, is used. The spectral values of absorption coefficient, α, and transport scattering coefficient, σ_{tr}, in a small volume containing monodisperse droplets are related with the efficiency factors as follows (the subscript λ is hereafter omitted for brevity) [7]:

$$\alpha = 0.75 f_v Q_a / a \qquad \sigma_{tr} = 0.75 f_v Q_s^{tr} / a \tag{7}$$

where f_v is the local volume fraction of droplets. It is convenient also to introduce the corresponding normalized coefficients $E_a = \alpha / f_v$ and $E_s^{tr} = \sigma_{tr} / f_v$.

It was shown in [7] that monodisperse approximation may lead to considerable errors in the case when particles of different size have different velocities and/or temperatures. Strictly speaking, more detailed calculations should be made to estimate these errors in the problem under consideration. It should be recalled that monodisperse approximation is inapplicable for thermal radiation calculations in the case of a strong difference in behaviour of particles of different size. The known examples are: the thermal radiation of particles in plasma spraying [33–36], the radiation from two-phase combustion products in exhaust plumes of aluminized-propellant rocket engines [37, 38], and the radiative cooling of core melt droplets in nuclear fuel-coolant interaction [39, 40]. Fortunately, the subsequent calculations showed that it is not the case for the problem under consideration and the monodisperse approximation is really applicable.

The calculated values of E_a and E_s^{tr} in the most important range of the problem parameters are presented in Fig. 4. It is clear that the radiation absorption by water droplets is significant in the absorption band of water. This absorption contributes to water evaporation and flame suppression. On the contrary, the scattering of the flame radiation by water droplets is more important outside the absorption band, where this effect is expected to be observed. It is interesting that spectral behaviour of both the absorption and transport scattering coefficients of droplets is similar for droplets of different sizes, but the scattering is much greater for relatively small droplets.

The present paper is focused on the radiation scattering by small water droplets. Therefore, the wavelength about 4 μm is the most interesting: the strong scattering of radiation by water droplets and relatively small absorption are typical for this spectral range (compare Figs. 4a and 4b).

The hypothesis of independent scattering does not work in the above obtained local areas of strong evaporation where the distance between the neighbouring droplets may be small as compared with both the droplet size and the radiation wavelength. According to [41–45], the dependent scattering may lead to significant changes in absorption and scattering characteristics of the turbulent gas flow with suspended clusters of closely spaced particles or droplets. One should recall papers [46–48], where this effect was observed and analysed as applied to cumulus clouds in the atmosphere. Of course, a study of this effect is a separate complex problem of both the physical optics and the turbulence of gas flows with suspended inertial particles and it is beyond the scope of the present paper. The ordinary relations for independent single droplets are used in subsequent estimates.

5. Approximate method for radiative transfer calculations

We use the known P_1 approximation of the spherical harmonics method [8, 49, 50] to estimate the effect of radiation scattering by water droplets on thermal radiation field in the flame. In our case, this approach leads to the following boundary-value problem for the modified Helmholtz equation:

$$-\nabla\left(D\nabla G\right)+\alpha G=4\pi\alpha_{\mathrm{g}}I_{\mathrm{b}}\left(T_{\mathrm{g}}\right)\qquad D=1/\left(3\beta_{\mathrm{tr}}\right)\qquad \alpha=\alpha_{\mathrm{g}}+\alpha_{\mathrm{d}} \tag{8a}$$

$$D\left(\vec{n}\cdot\nabla G\right)=\frac{\varepsilon_{\mathrm{w}}}{2\left(2-\varepsilon_{\mathrm{w}}\right)}\left(G-4\pi I_{\mathrm{b}}\left(T_{\mathrm{w}}\right)\right) \tag{8b}$$

where $G=\int\limits_{(4\pi)} I\,\mathrm{d}\vec{\Omega}$ is the irradiation function, D is the so-called radiation diffusion coefficient, $\beta_{\mathrm{tr}}=\alpha+\sigma_{\mathrm{s}}^{\mathrm{tr}}$ is the transport extinction coefficient, α_{g} and α_{d} are the absorption coefficients of a gas medium and suspended water droplets, $\vec{n}$ is the external normal to the boundary of the computational region. Of course, the spectral irradiation G, the gas temperature T_{g}, and all physical coefficients in Eq. (8a) are the functions of spatial coordinates. The Marshak boundary condition (8b) contains the temperature, T_{w}, and hemispherical emissivity, ε_{w}, on boundary surfaces. Obviously, one should formally put $\varepsilon_{\mathrm{w}}=1$ and $T_{\mathrm{w}}=0$ at the open surface of the flame. It means that there is no any external

radiation at these boundaries. After obtaining the P_1 solution, the spectral component of the radiation power generated in the flame is expressed as follows:

$$W = 4\pi\alpha_{\mathrm{g}} I_{\mathrm{b}}\left(T_{\mathrm{g}}\right) - \alpha G \tag{9}$$

The P_1 approximation is simple and very convenient for radiative transfer calculations especially in combined heat transfer problems. Moreover, this approach appears to be sufficiently accurate in the case when one needs only the divergence of radiative flux, $W_{\mathrm{t}} = \int W \mathrm{d}\lambda$, which is an important term in the energy equation [51–54]. At the same time, the radiative flux calculations at the boundaries of the computational region using the P_1 may lead to significant errors. A physical analysis of these errors has been made in early paper [55] and can be found also in monograph [7]. This drawback of P_1 can be compensated with the use of the combined two-step method and transport approximation for the scattering phase function, when the P_1 is employed in CFD calculations only, whereas a ray-tracing procedure is used to solve the spectral radiative transfer equation at the second step of the complete solution [7, 56–59]:

$$\vec{\Omega}\nabla I + \beta_{\mathrm{tr}} I = S \qquad S = \frac{\sigma_{\mathrm{s}}^{\mathrm{tr}}}{4\pi} G + \alpha_{\mathrm{g}} I_{\mathrm{b}}\left(T_{\mathrm{g}}\right) \tag{10}$$

where S is the so-called source function. However, the ray-tracing calculations are not necessary in the present paper because we are just going to compare several variants to estimate an effect of infrared scattering on the radiation field in the flame. According to [7, 58, 59], the finite-element method [60] with the simplest linear presentation of function G in triangular finite elements is used to solve a variational formulation of the P_1 boundary-value problem.

6. Effect of infrared scattering by evaporating water droplets

There is no need for complete calculations over the spectrum to estimate qualitatively the effect of infrared scattering by evaporating water droplets in the above described example pool fire. It is sufficient to consider spectral results at the representative wavelength of $\lambda = 4.2\,\mu\mathrm{m}$, near the peak of the CO_2 absorption band. The radiation absorption by droplets is relatively small in this range but $E_{\mathrm{s}}^{\mathrm{tr}} \approx 300\,\mathrm{cm}^{-1}$ at $a = 10\,\mu\mathrm{m}$ and 1000 cm^{-1} at $a = 5\,\mu\mathrm{m}$ (see Fig. 4b). In the computational estimates, the following conventional circular regions containing small water droplets are considered:

$$r < 5\,\mathrm{cm},\ 30 < z < 50\,\mathrm{cm} - \text{for droplets with } a = 10\,\mu\mathrm{m} \tag{11a}$$

$$5 < r < 15\,\mathrm{cm},\ 45 < z < 50\,\mathrm{cm} - \text{for droplets with } a = 5\,\mu\mathrm{m} \tag{11b}$$

It is assumed that the monodisperse small droplets are uniformly distributed in these sub-regions. Of course, equations (11a) and (11b) should be considered as a crude preliminary estimate only because the real size and spatial distributions of evaporating small droplets are smooth. The estimate of the infrared scattering effect can be obtained by comparison of two variants of volume fraction of droplets: $f_{\mathrm{v}} = 0$ (no droplets) and $f_{\mathrm{v}} = 5 \cdot 10^{-4}$. One can consider the numerical data for the fields of normalized dimensionless irradiation as it was done in paper [6]:

$$\overline{G} = \frac{G}{\pi I_{\mathrm{b}}(T_{\mathrm{ref}})} \tag{12}$$

The irradiation value is really important to estimate an additional evaporation of water droplets due to absorption of thermal radiation. However, it is more interesting to analyse the normalized source functions, $\overline{S}$, because this function is used in the subsequent ray-tracing calculations of the spectral radiative flux observed at arbitrary point outside the flame [7]:

$$\overline{S} = \frac{S}{I_{\mathrm{b}}(T_{\mathrm{ref}})} = \alpha_{\mathrm{g}} \frac{I_{\mathrm{b}}(T_{\mathrm{g}})}{I_{\mathrm{b}}(T_{\mathrm{ref}})} + \frac{\sigma_{\mathrm{tr}} \overline{G}}{4} \tag{13}$$

The values of $T_{\mathrm{ref}} = 1000\,\mathrm{K}$ and the emissivity of the liquid fuel surface $\varepsilon_{\mathrm{w}} = 0.6$ [61] were used in the calculations. The latter does not mean that thermal radiation of relatively cold liquid fuel is important. However, we take into account a partial reflection of the flame radiation from the surface of liquid fuel.

Note that the value of $\overline{S}$ is measured in m^{-1}. The following analytical relation was used for the profile of side boundary of the computational region:

$$r = r_{\max} - \xi (z - z_1)^2 \qquad r_{\max} = 0.35\,\mathrm{m} \qquad z_1 = 0.25\,\mathrm{m} \qquad \xi = 3.2\,\mathrm{m}^{-1} \tag{14}$$

The non-uniform triangulation of the computational region with 1600 elements is shown in Fig. 5. The smaller areas of finite elements were made in the region of more optically dense medium. As usually, the radial coordinates of all the nodes were increased by the first radial interval of the mesh to avoid the formal difficulties in numerical calculations near the axis [7]. The calculated fields of function $\overline{S}$ in the most interesting part of the fire cross section are presented in Fig. 6. The circular regions (11) containing fast evaporating and almost immovable water droplets can be simply identified near the right-hand boundary and at the lower panel of Fig. 6b because of a considerable contribution of scattering to the radiative source function. Of course, there are no sharp edges of these areas in reality. One should use more accurate data for evaporating droplets to obtain smooth boundaries of the scattering region in the

radiation calculations. However, the latter is not necessary for the qualitative estimates of the present paper. It is important that strong infrared scattering in local areas of small evaporating water droplets is physically sound and it is confirmed by direct calculations. To the best of our knowledge, this effect is computationally obtained for the first time.

7. Conclusion

The scattering of infrared radiation of a developing pool fire by evaporating water droplets in fire suppression by water sprays was predicted on the basis of theoretical and computational estimates. It was shown for the first time that small evaporating droplets with different initial size can be focused in local areas of the flame before their total evaporation. The calculations for real developing flame showed that the effect of infrared radiation scattering by almost immovable and fast evaporating water droplets on the radiation field in the flame and also on the source function responsible for the infrared radiation from the flame is considerable. The latter can be observed at the initial stage of fire suppression using the probe water sprays supplied from above. This new finding should be taken into account in further studies of suppression of open flames by water sprays. It is important that positions of the local highly-scattering regions and the expected motions of these regions are very sensitive to flame parameters. This can be used in probe experiments for partial validation of transient CFD simulations.

Acknowledgments

The authors gratefully acknowledge the financial support by the H2020-MSCA-IF-2016 Programme of the European Commission (RAD-FIRE project, number 749220). We also wish to thank Ivan Sikic and Antoine Hubert for the CFD calculation and kind assistance in processing the pool fire data.

REFERNCES

[1] Tatem PA, Beyley CL, DiNenno PJ, Budnick EK, Back GG, Younis SE. A review of water mist technology for fire suppression., Naval Research Laboratory. 1994. NRL/MR/6180-94-7624.

[2] Dembele S, Tam VHY, Ferrais S, Rosario RAF, Wen JF. Effectiveness of water deluge in fire suppression and mitigation. IChemE Symposium Series No. 153. 2007. 8 pp.

[3] Yu HZ. Physical scaling of water mist suppression of pool fires in enclosures. Fire Safety J. 2011; 10: 145–158.

[4] Gupta M, Pasi A, Ray A, Kale SR. An experimental study of the effects of water mist characteristics on pool fire suppression. Exper. Thermal Fluid Sci. 2013; 44: 768–778.

[5] Jenft A, Collin A, Boulet A, Pianet G, Breton A, Muller BA. Experimental and numerical study of pool fire suppression using water mist. Fire Safety J. 2014; 67: 1–12.

[6] Dombrovsky LA, Dembele S, Wen JX, Sikic I. Suppression of pool fires by water sprays: The effect of light scattering by evaporating droplets, Proc. 6th Int. Conf. Comput. Thermal Radiation in Participating Media (CTRPM-VI), April 9-11. Cascais, Portugal, 2018, paper 30.

[7] Dombrovsky LA and Baillis D. Thermal Radiation in Disperse Systems: An Engineering Approach. New York: Begell House, 2010.

[8] Dombrovsky LA, Dembele S, Wen JX. A simplified model for the shielding of fire thermal radiation by water mists. Int. J. Heat Mass Transfer. 2016; 96: 199–209.

[9] Dombrovsky LA, Dembele S, Wen JX. Shielding of fire radiation with the use of multi-layered mist curtains: Preliminary estimates. Comput. Thermal Sci. 2016; 8: 371–80.

[10] Jensen KA, Suo-Anttila JM, Blevins LG. Measurement of soot morphology, chemistry, and optical properties in the visible and near-infrared spectrum in the flame zone and overfire region of large JP-8 pool fires. Combust. Sci. Technol. 2007; 179: 2453–87.

[11] Liu L, Mishchenko MI, Arnott WP. A study of radiative properties of fractal soot aggregates using the superposition T-matrix method. J. Quant. Spectr. Radiat. Transfer. 2008; 109: 2656–63.

[12] Liu F, Wong C, Snelling D, Smallwood GJ. Investigation of absorption and scattering properties of soot aggregates of different fractal dimension at 532 nm using RDG and GMM. Aerosol Sci. Technol. 2013; 47: 1393–405.

[13] Doner N and Liu F. Impact of morphology on the radiative properties of fractal soot aggregates. J. Quant. Spectr. Radiat. Transfer. 2017; 187: 10–9.

[14] Downie B, Polymeropoulos C, Godos G. Interaction of a water mist buoyant methane diffusion flame. Fire Safety J. 1995; 24: 359–81.

[15] Prasad K, Liu C, Kailasanath K. Simulation of water mist suppression of small scale methanol liquid fires. Fire Safety J. 1999; 33: 185–212.

[16] Hua J, Kumar K, Khoo DC, Xue H. A numerical study of the interaction of water spray with fire plume. Fire Safety J. 2002; 37: 631–57.

[17] Beji T, Zadeh SE, Maragkos G, Merci B. Influence of droplet size distribution and volume fraction angular distribution on the results and computational time of water spray CFD simulations. Fire Safety J. 2017; 91: 586–95.

[18] Floid J and McDermont R. Development and evaluation of two new droplet evaporation schemes for fire dynamics simulations. Fire Safety J. 2017; 91: 643–52.

[19] Crowe CT, Schwarzkopf JD, Sommerfeld M, Tsuji Y. Multiphase Flows with Droplets and Particles, Second edition. New York: CRC Press, 2011.

[20] Kryukov AP, Levashov VYu, Shishkova IN. Evaporation in mixture of vapour and gas mixture. Int. J. Heat Mass Transfer. 2009; 52: 5585–90.

[21] Dombrovsky LA, Reviznikov DL, Kryukov AP, Levashov VYu. Self-generated clouds of micron-sized particles as a promising way of a Solar Probe shielding from intense thermal radiation of the Sun. J. Quant. Spectr. Radiat. Transfer. 2017; 200: 234–43.

[22] Eaton JK and Fessler JR. Preferential concentration of particles by turbulence. Int. J. Heat Mass Transfer. 1994; 20 (Suppl. 1): 169–209.

[23] Zaichik LI and Alipchenkov VM. Pair dispersion and preferential concentration of particles in isotropic turbulence. Phys. Fluids. 2003; 15:1776–87.

[24] Uhlmann M and Chouippe A. Clustering and preferential concentration of finite-size particles in forced homogeneous-isotropic turbulence. J. Fluid Mech. 2017; 812: 991–1023.

[25] Hale GM and Querry MP. Optical constants of water in the 200 nm to 200 μm wavelength region. Appl. Optics. 1973; 12: 555–63.

[26] Zolotarev VM and Dyomin AV. Optical constants of water in wide wavelength range 0.1Å÷1m. Optics Spectr. 1977; 43: 271–9.

[27] van de Hulst HC. Light Scattering by Small Particles. New York: Dover, 1981.

[28] Bohren CF and Huffman DR. Absorption and Scattering of Light by Small Particles. New York: Wiley, 1983.

[29] Hergert W and Wriedt T. The Mie Theory: Basics and Applications. Berlin: Springer, 2012.

[30] Dombrovsky LA. Spectral model of absorption and scattering of thermal radiation by diesel fuel droplets. High Temperature. 2002; 40: 242–8.

[31] Born M and Wolf E. Principles of Optics. Seventh (expanded) edition. New York: Cambridge Univ. Press, 1999.

[32] Hancer M, Sperline RP, Miller JD. Anomalous dispersion effects in the IR-ATR spectroscopy of water. Appl. Spectr. 2000; 54: 133–43.

[33] Dombrovsky LA and Ignatiev MB. An estimate of the temperature of semitransparent oxide particles in thermal spraying. Heat Transfer Eng. 2003; 24: 60–8.

[34] Fauchais P, Montavon G, Bertrand G. From powders to thermally sprayed coatings. J. Therm. Spray Technol. 2010; 19: 56–80.

[35] Fauchais PL, Heberlein VR, Boulos MI. Thermal Spray Fundamentals: From Powder to Part. New York: Springer, 2014.

[36] Chazelas C, Trelles JP, Cjouquet I, Vardelle A. Main issues for fully predictive spray torch model and numerical considerations. Plasma Chem. Plasma Proc. 2017; 37: 627–51.

[37] Cai G, Zhu D, Zhang X. Numerical simulation of the infrared radiative signatures of liquid and solid rocket plumes. Aerospace Sci. Technol. 2007; 11: 473–80.

[38] Binauld Q, Lamet J-M, Tessé L, Rivière P, Soufiani A. Numerical simulation of radiation in high altitude solid propellant rocket plumes. Proc. 7th European Conf. Aeronautics & Aerospace Sci. (EUCASS). 2017; paper EUCASS2017-441.

[39] Dombrovsky LA. Large-cell model of radiation heat transfer in multiphase flows typical for fuel–coolant interaction. Int. J. Heat Mass Transfer 2007; 50: 3401–10.

[40] Dombrovsky LA, Davydov MV, Kudinov P. Thermal radiation modeling in numerical simulation of melt–coolant interaction. Comput. Thermal Sci. 2009; 1: 1–35.

[41] Mishchenko MI, Travis LD, Lacis AA. Multiple Scattering of Light by Particles: Radiative Transfer and Coherent Backscattering, Cambridge (UK): Cambridge Univ. Press, 2006.

[42] Doicu A, Wriedt T, Eremin YA. Light Scattering by System of Particles. Berlin: Springer, 2006.

[43] Okada Y and Kokhanovsky AA. Light scattering and absorption by densely packed groups of spherical particles. J. Quant. Spectr. Radiat. Transfer. 2009; 110: 902–917.

[44] Mishchenko MI. Electromagnetic Scattering by Particles and Particle Groups: An Introduction. Cambridge (UK): Cambridge Univ. Press, 2014.

[45] Ma LX, Tan JY, Zhao JM, Wang FQ, Wang CA. Multiple and dependent scattering by densely packed discrete spheres: Comparison of radiative transfer and Maxwell theory. J. Quant. Spectr. Radiat. Transfer. 2017; 187: 255–66.

[46] Erkelens JS, Venema VKS, Russchenberg HWJ, Ligthart LP. Coherent scattering of microwaves by particles: Evidence from clouds and smoke. J. Atmos. Sci. 2001; 58: 1091–102.

[47] Shaw RA. Particle-turbulence interactions in atmospheric clouds. Ann. Rev. Fluid Mech. 2003; 35: 183–227.

[48] Dombrovsky LA and Zaichik LI. An effect of turbulent clustering on scattering of microwave radiation by small particles in the atmosphere. J. Quant. Spectr. Radiat. Transfer. 2010; 111: 234–42.

[49] Howell JR, Siegel R, Mengüç MP. Thermal Radiation Heat Transfer, New York: CRC Press, 2010.

[50] Modest MF. Radiative Heat Transfer, Third edition. New York: Acad. Press, 2013.

[51] Viskanta R. Radiative Transfer in Combustion Systems: Fundamentals and Applications. New York: Begell House, 2005.

[52] Li G and Modest MF. A method to accelerate convergence and to preserve radiative energy balance in solving the P_1 equation by iterative methods. ASME J. Heat Transfer. 2002; 124: 580–2.

[53] Kontogeorgos DA, Keramida EP, Founti MA. Assessment of simplified thermal radiation models for engineering calculations in natural gas-fired furnace. Int. J. Heat Mass Transfer. 2007; 50: 5260–8.

[54] Sun Y and Zhang X., Contribution of gray gases in SLW for non-gray radiation heat transfer and corresponding accuracies of FVM and P1 method. Int. J. Heat Mass Transfer. 2018; 121: 819–31.

[55] Dombrovsky LA, Evaluation of the error of the P_1 approximation in calculations of thermal radiation transfer in optically inhomogeneous media, High Temperature. 1997; 35: 676–9.

[56] Dombrovsky LA. Approximate methods for calculating radiation heat transfer in dispersed systems. Thermal Engineering. 1996; 43: 235–43.

[57] Dombrovsky LA. The use of transport approximation and diffusion-based models in radiative transfer calculations. Comput. Thermal Sci. 2012; 4: 297–315.

[58] Dombrovsky LA and Lipiński W. A combined P_1 and Monte Carlo model for multi-dimensional radiative transfer problems in scattering media, Comput. Thermal Sci. 2010; 2: 549–60.

[59] Dombrovsky LA, Reviznikov DL, Sposobin AV. Radiative heat transfer from supersonic flow with suspended particles to a blunt body. Int. J. Heat Mass Transfer. 2016; 93: 853–61.

[60] Zienkiewicz OC, Taylor RL, Zhu JZ. The Finite Element Method: Its Basis and Fundamentals, Seventh Edition. New York: Elsevier, 2015.

[61] Snegirev AYu. Statistical modelling of thermal radiation transfer in buoyant turbulent diffusion flames. Combust. Flame. 2004; 136: 51–71.

Figure captions

Figure 1. Parameters of the transient model flame [1]: (a) – the gas temperature field; (b), (c) – the profiles of axial component of gas velocity and gas temperature.

Figure 2. Variation of droplet radius along the focusing trajectories at two initial positions of water droplets: (a) $r_0 = 0$ ($u_{d0} = 2 - 5$ m/s) and (b) $r_0 = 0.1$ m ($u_{d0} = 10$ m/s).

Figure 3. Spectral indices of refraction (a) and absorption (b) of pure water.

Figure 4. Normalized (a) absorption and (b) transport scattering coefficients of water droplets.

Figure 5. Finite-element triangulation of the flame computational region, which includes the main part of the temperature field shown in Fig. 1. The left boundary of the region is the surface of a liquid fuel.

Figure 6. Normalized spectral source function at the wavelength of $\lambda = 4.2$ μm: a – without water droplets, b – with water droplets.

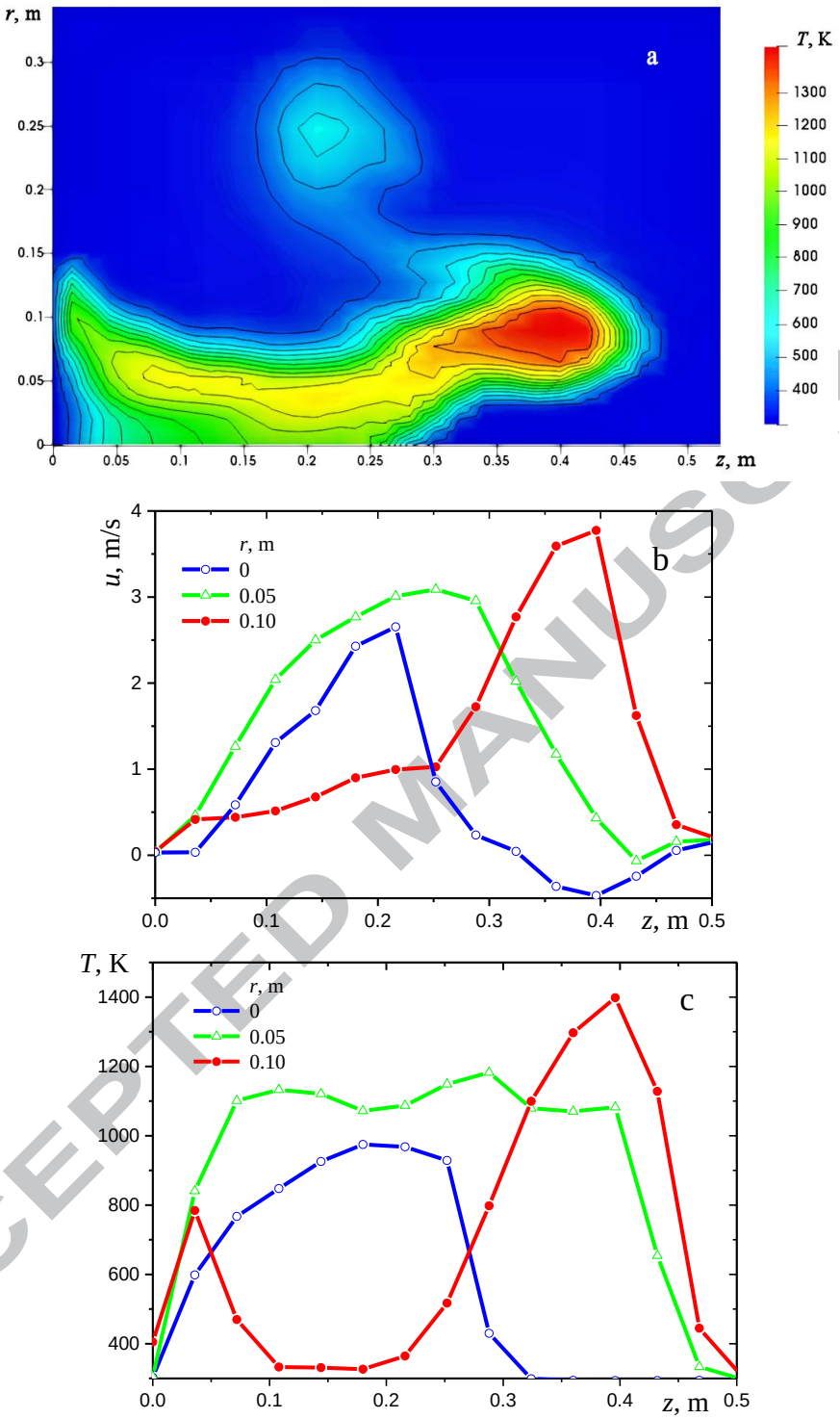

Figure 1

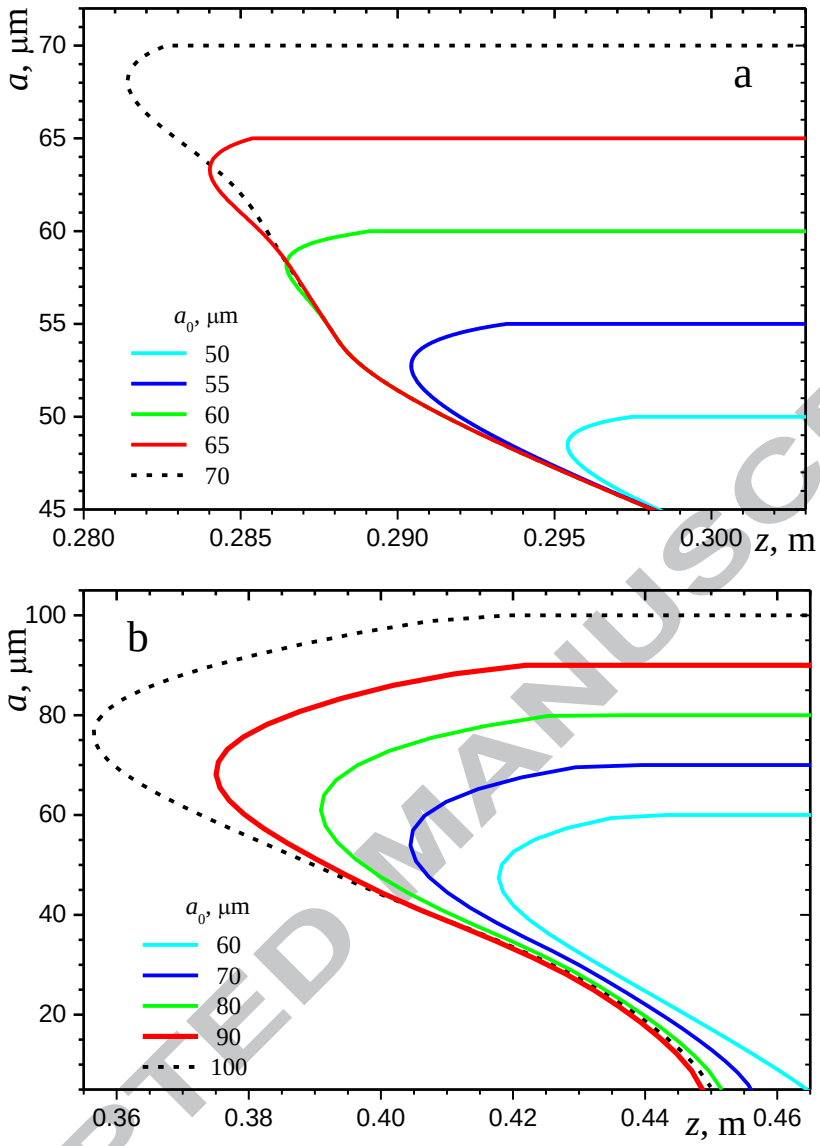

Figure 2

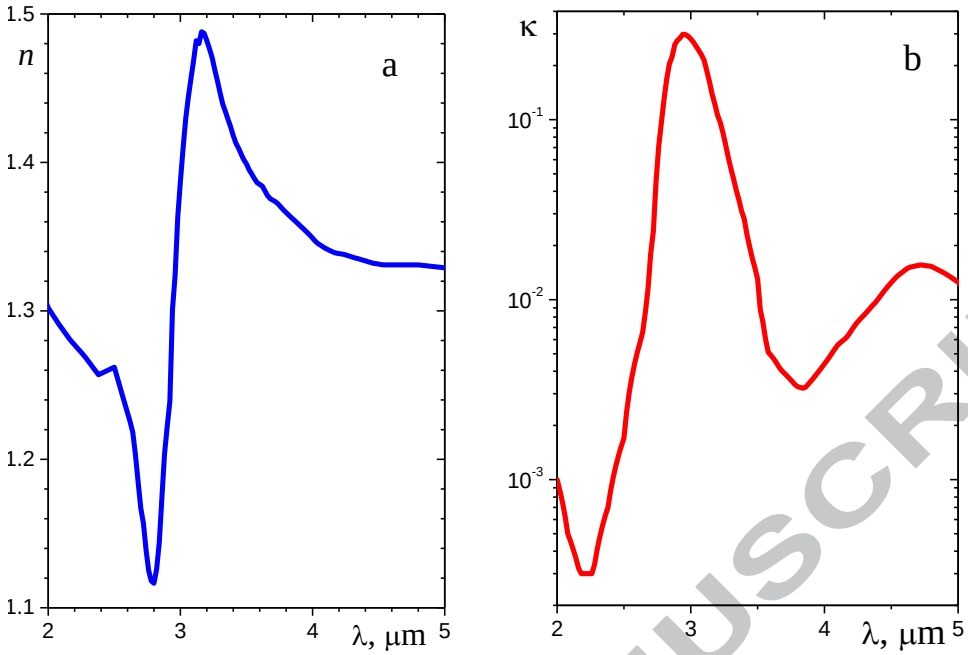

Figure 3

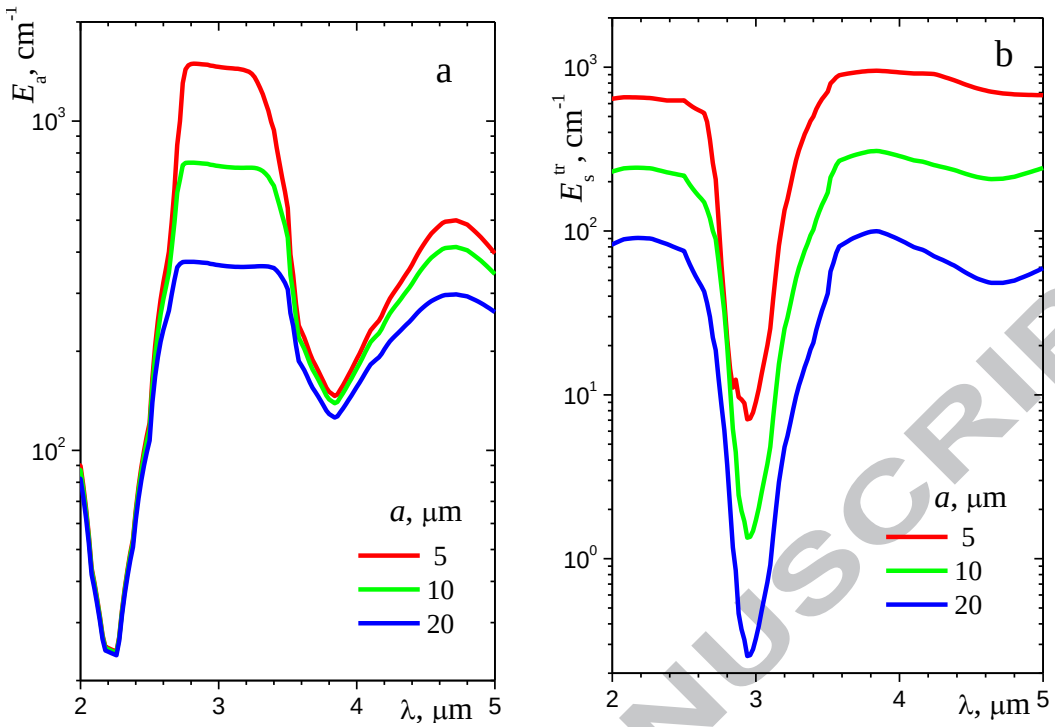

Figure 4

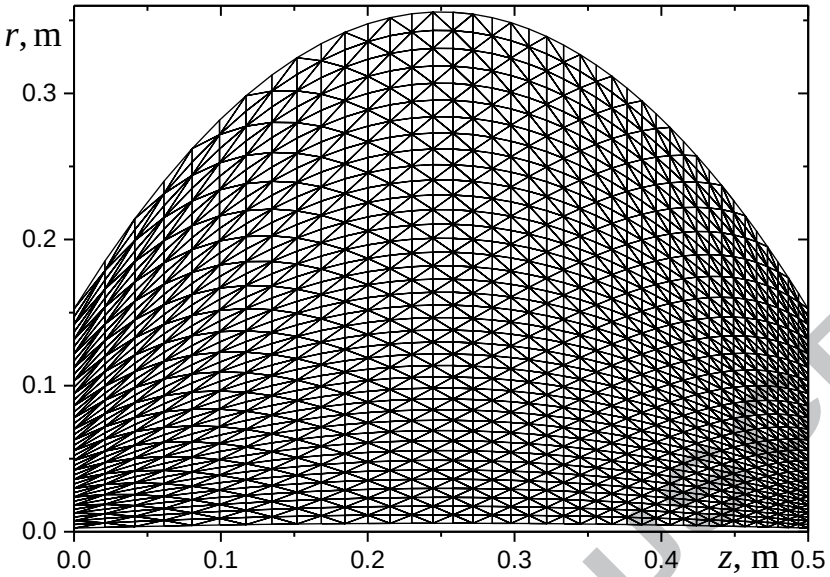

Figure 5

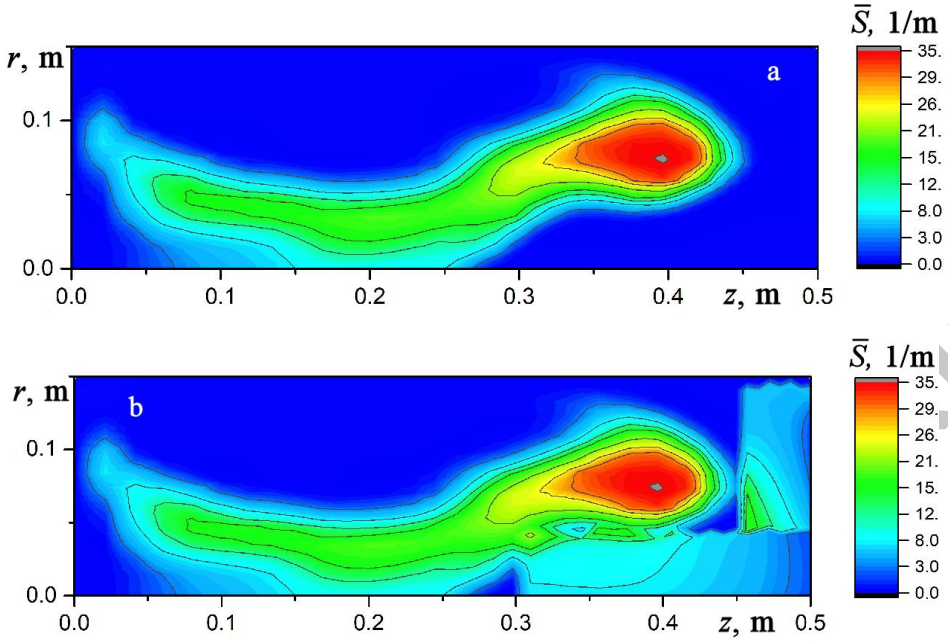

Figure 6

- An initial stage of a pool fire suppression is considered.
- The motion, heating, and evaporation of water droplets are calculated.
- Focusing of evaporating water droplets in local regions is obtained.
- A strong infrared scattering by small water droplets is analyzed.
- The spectral region of a significant infrared scattering is determined.
- The use of the infrared scattering in flame observations is discussed.